Journal of Molecular Liquids 318 (2020) 114066

Contents lists available at ScienceDirect

Journal of Molecular Liquids

journal homepage: www.elsevier.com/locate/molliq

Chitosan-graphene oxide nanocomposites as water-solubilising agents for rotenone pesticide

Mohd Sahli Muda [a], Azlan Kamari [a,*], Suriani Abu Bakar [b], Siti Najiah Mohd Yusoff [a], Is Fatimah [c], Esther Phillip [d], Shahrulnizahana Mohammad Din [e]

[a] Department of Chemistry, Faculty Science and Mathematics, Universiti Pendidikan Sultan Idris, 35900 Tanjong Malim, Perak, Malaysia
[b] Department of Physics, Faculty Science and Mathematics, Universiti Pendidikan Sultan Idris, 35900 Tanjong Malim, Perak, Malaysia
[c] Department of Chemistry, Faculty of Mathematics and Natural Sciences, Universitas Islam Indonesia, Yogyakarta 55584, Indonesia
[d] Malaysian Nuclear Agency, Bangi, 43000 Kajang, Selangor, Malaysia
[e] Department of Chemistry, Johore State, Jalan Abdul Samad, 80100 Johor Bahru, Johor, Malaysia

ARTICLE INFO

Article history:
Received 7 May 2020
Received in revised form 1 August 2020
Accepted 13 August 2020
Available online 16 August 2020

Keywords:
Chitosan-graphene oxide nanocomposite
Rotenone pesticide
Water-solubilising agent
Nanocarrier
Adsorption process
Interaction mechanism

ABSTRACT

In the present work, the feasibility of chitosan-graphene oxide (CS-GO) nanocomposites, namely CS-GO 1% (w/w), CS-GO 2% (w/w) and CS-GO 3% (w/w) as water-solubilising agents for rotenone pesticide was evaluated for the first time. The CS-GO nanocomposites were characterised by using FTIR, SEM, TEM and XRD analyses. The interaction of nanocomposites with rotenone was investigated through adsorption study involving several experimental parameters such as solution pH, initial concentration and contact time. Additionally, the desorption study was carried out using HCl and NaOH as desorption agents. Based on correlation coefficient (R^2), the adsorption kinetic data were best described by the pseudo-first order equation while the adsorption equilibrium data were correlated well with the Langmuir isotherm model. The GO nanoparticle aggregates have a spherical shape with size ranged from 1.40 to 34.7 nm. The crystallinity of CS was increased following interaction with GO, whereby the intensity of diffractive peak at $2\theta = 20.42°$ was increased to more than 4000 counts. Based on Langmuir isotherm model, CS-GO 3% (w/w) exhibited the highest adsorption capacity for rotenone with Q value of 92.59 mg/g. The main mechanism for interaction of CS-GO nanocomposites with rotenone was through formation of hydrogen bond. The presence of -OH, -COOH and -NH functional groups on CS-GO nanocomposites significantly contributed to water-solubilising mechanism. The CS-GO 1% (w/w), CS-GO 2% (w/w) and CS-GO 3% (w/w) nanocomposites were able to increase the solubility of rotenone in water by 34.40%, 38.80% and 46.30%, respectively.

1. Introduction

Biopesticides have received great attention from scientists as promising alternatives to chemical pesticides mainly because they comprised of plant-derived active ingredients to control pests and pathogens [1]. Unfortunately, most of the plant origin active ingredients are hydrophobic compounds thus limit the production of botanical pesticides [2]. The usage of large amount of organic solvents to dissolve hydrophobic active ingredients in pesticide formulations had significantly polluted the environment [3]. This scenario has created opportunities to scientists to develop eco-friendly pesticides through application of materials that are able to act as water-solubilising carrier agents [4].

Carrier agents are purposely designated for the protection of pesticides by increasing their chemical stability when opposed the harsh environmental conditions such as high temperature and radiation [5]. In the context of active ingredients, the carrier agents will protect them before their target-specific release, improve their solubility and penetration, and control the release functions of active ingredients into the surrounding environment [6]. There are several binding mechanisms for carrier agents, namely encapsulation, entrapment, adsorption and through ligands [7].

Graphene oxide (GO) is composed of a single-atom-thick lattice of honeycomb-like sp^2-bonded carbon atoms, possesses plenty of oxygen-containing polar functionalities such as carbonyl, epoxide, carboxyl and hydroxyl groups [8]. The abundance of oxygen functionalities presence in GO enables it to disperse more easily in organic solvents, water and different matrices. The potential application of GO in delivery of hydrophobic pesticides, namely chlorpyrifos, endosulfan, and malathion has been investigated by several researchers. GO was reported to exhibit a spontaneous adsorption interaction with the three pesticides studied [9].

Designed with the composition of β-(1–4)-linked-2-2-deoxy-2-amino-D-glucopyranose, chitosan (CS) is comprised with plenty of chelating groups including primary and secondary hydroxyl groups, along

* Corresponding author.
E-mail address: azlan.kamari@fsmt.upsi.edu.my (A. Kamari).

https://doi.org/10.1016/j.molliq.2020.114066
0167-7322/

with highly reactive amino groups [10]. CS has been used in drug delivery for medical application. Biological adhesiveness of CS can promote drug permeability, for the benefit of drug delivery carrier from nasal to brain [11]. Among the various biopolymers researched, CS has been regarded to have excellent potential for delivery applications.

Rotenone or also known as (1,2,12,12a-tetrahydro-8,9-dimethoxy-2-(1-methyl-ethenyl)-1-benzopyrano[3,5-*b*]furo[2,3-*h*]benzopyran-6(6h)-one) [12], is a rotenoid ester and naturally occurring compound derived from the constituents of the roots, leaves and stems of many botanical species of the genera Derris, Amorpha, Tephrosia and Lonchocarpus [13]. Rotenone has been legally used in organic crop production owing to its natural origin and lack persistence in the environment. Hence, it is readily degrades to form water and dihydrorotenone [14]. In addition, it is extremely toxic to pest such as corn borers, apple and pea aphids, Mexican bean beetles, and household pests, but moderately non-toxic to mammals and plants [3]. Upon contact with water, rotenone undergoes several chemical reactions including oxidation, hydrolysis and photochemical conversion. Rotenone is nearly insoluble in water approximately 0.002 mg/mL at 20 °C [3].

Kamari et al. [15] have reported the successful of *N*,*N*-dimethylhexadecyl carboxymethyl chitosan (DCMC) as amphiphilic water-solubilising agent for rotenone pesticide In their study, the designated nanocomposite was able to increase the water solubility of rotenone up to 48.5 times than free rotenone in water. The overall aim of this work is to prepare, characterise and evaluate the potential of CS-GO nanocomposites to bind hydrophobic rotenone pesticide in water. To the best of our knowledge, this is the first attempt to study the interaction mechanism between CS-GO nanocomposites and rotenone in water environment.

2. Materials and methods

2.1. Materials

CS derived from shrimp shells (99% deacetylated, MW 33 kDa) was supplied by Sigma-Aldrich. GO (with 99% purity) was purchased from HmBG Reagent Chemicals and glutaraldehyde was acquired from Merck. All chemicals were of analytical grade and used as received without further purification.

2.2. Preparation of CS-GO nanocomposites

CS-GO nanocomposites were prepared following to the procedure outlined by Fan et al. [16] with some modifications. Three CS-GO nanocomposites were synthesised by modifying the weight ratio of CS to GO and coded as CS-GO 1% (w/w), CS-GO 2% (w/w) and CS-GO 3% (w/w). To prepare CS-GO 1% (w/w), 0.2 g of CS was dissolved in 1% (v/v) acetic acid solution at room temperature (25 °C). GO (0.2 g) was then added into the suspension and stirred vigorously for 30 min by using a magnetic stirrer to obtain a homogenous dispersion. The CS-GO mixture was sonicated with an ultrasonic sonicator for 90 min at 60 °C to remove gas bubble. After sonication process, the pH of CS-GO suspension was adjusted to 9–10 by adding NaOH (1% v/v) to precipitate the CS-GO. The precipitate was heated at 60 °C for 60 min in an oven. Then, 2 mL of glutaraldehyde was added into the reaction mixture for cross-linking of CS and continuously stirred for another 30 min. Following centrifugation process, black product was collected and rinsed with diluted acetic acid and deionised water to remove the unreacted CS. The black powder was dried at 60 °C overnight. The experiment was repeated by using 0.4 g and 0.6 g of GO in order to produce CS-GO 2% (w/w) and CS-GO 3% (w/w), respectively.

2.3. Characterisation study

2.3.1. Fourier transform infrared (FTIR) spectroscopy analysis

The presence of functional groups and potential reactive sites of the nanocomposites was investigated by using a Thermo Nicolet 6700 FTIR Spectrometer with over 30 cumulative scans in the wavenumber ranged between 400 and 4000 cm^{-1}. A pallet of each nanocomposite was prepared with a weight ratio of 1:10 (nanocomposite:KBr), separately.

2.3.2. CHNO elemental analysis

The percentage of C, H, N and O in each nanocomposite was analysed by using a CHNS-O Flash EA 1112 Series Elemental Analyser. Approximately, 2.0 mg of nanocomposite was weighed in a tin capsule and then transferred into a reactor for combustion process. Acetanilide, oxygen and helium were used as standard, oxidant and carrier gas, respectively.

2.3.3. Scanning electron microscopy (SEM) analysis

SEM analysis was conducted in order to observe the surface morphology of CS before and after interaction with GO. The CS-GO nanocomposites were first coated with platinum to avoid electron charging by using Automatic Platinum Sputter Coater System (Quorum Q150RS). The SEM analysis was performed on a Hitachi SU 8020 UHC Field Emission Scanning Electron Microscope (FESEM) set at accelerating voltage of 2.0 to 5.0 kV. The surface morphology of the nanocomposites was observed at several magnifications.

2.3.4. Transmission electron microscopy (TEM) analysis

The internal morphology of each nanocomposite was observed at several magnifications. About 8.0 mg of nanocomposite was dissolved in 2.0 mL of deionised water followed by 2.0 mL of acetone. The solution was treated with ultrasound for 20 min, before two drops of sample solution were dropped on the copper grid and left for drying process under room temperature. TEM analysis was performed at 30.0 kV using a tungsten filament.

2.3.5. X-ray diffraction (XRD) spectroscopy analysis

The change in crystalline structure of CS following introduction of GO was examined by using a Shimadzu X-ray Diffractometer 6000 equipped with Lynx eye high speed detector. The instrument was equipped with Cu-Kα radiation of 1.5406 nm. The XRD patterns were recorded over 2θ region of 0 to 100° with a scanning speed set at 2° per minutes.

2.4. Performance study

2.4.1. Solubility study

The correlation of the pH dependence towards water solubility of each nanocomposite was studied from measurement of transmittance of each solution. In this study, 10 mg of each CS-GO nanocomposite was dissolved in 10 mL of 2% (v/v) HCl solution. The pH of solution was varied from 1 to 13 by the addition of different molarity of NaOH solution. The transmittance of the solutions was analysed at 600 nm by using an Agilent Cary 60 UV–Visible Spectrophotometer.

2.4.2. Adsorption study

The potential of CS-GO nanocomposites to adsorb rotenone was evaluated in batch adsorption experiments, which involved several experimental parameters. Briefly, after adsorption process the solutions were filtered through Filter Fioroni (125 mm) filter paper. The residual rotenone concentration was measured by using UV–Visible spectrophotometer. All experiments were conducted in triplicates and average values (with respective standard error of average) are reported. The acetone and ethanol (1:1 v/v) blanks were used as controls.

The adsorption capacity of rotenone towards CS-GO nanocomposite was calculated by using Eq. (1) [4]:

$$qe = \frac{(Co - Ce)V}{W} \quad (1)$$

where *qe* (mg/g) is the adsorption capacity of the rotenone at equilibrium, *Co* and *Ce* (mg/L) are the initial and equilibrium concentration

of rotenone respectively. V (L) refers to the volume of rotenone solution and W (g) represents the weight of CS-GO nanocomposite.

The effect of solution pH on rotenone adsorption was studied between pH 1 to 9. In this experiment, the initial pH of solution was adjusted by using 0.1 mol/L of HCl and 0.1 mol/L of NaOH. The pH value was measured by using a Thermo Scientific Orion 2-star pH meter.

The effect of contact time was carried out with 10 mL of rotenone solution at 50 mg/L concentration in 250 mL conical flasks. The samples were equilibrated by shaking at predetermined times (15 to 90 min) at 100 rpm for 60 min by using a protech Orbital Shaker (model 720).

The effect of initial concentration of rotenone solution was investigated in the concentration range of 10 to 100 mg/L.

2.4.3. Adsorption kinetic study

Adsorption kinetic is fundamental in predicting the adsorption rate for designing and modeling the adsorption process. In this study, the kinetic data were fitted to pseudo-first order (Eq. (2)) [17], pseudo-second order (Eq. (3)) [18] and intraparticle diffusion (Eq. (4)) [19] kinetic models in order to understand the adsorption mechanism.

$$\log(q_e - q_t) = \log q_e - \frac{k1}{2.303}t \tag{2}$$

$$\frac{t}{qt} = \frac{1}{k2qe^2} + \frac{t}{qe} \tag{3}$$

$$q_t = C + kid\sqrt{t} \tag{4}$$

where qe (mg/g) and qt (mg/g) are the amount of rotenone adsorbed onto CS-GO nanocomposite at equilibrium tand contact time t, respectively. Meanwhile, k_1 (1/min), k_2 (g/mg min) and kid (mg/g $\text{min}^{0.5}$) are the rate constants for pseudo-first order, pseudo-second order and intraparticle diffusion, respectively. C is the constant and the selection of the best fitting kinetic model was based on the highest correlation coefficient (R^2).

2.4.4. Adsorption isotherm study

The interaction behaviour between rotenone and CS-GO surfaces was further studied. The equilibrium adsorption data were correlated with the Langmuir and Freundlich isotherm models. The linearised Langmuir equation is expressed in the Eq. (5) [20], while the linearised Freundlich equation is calculated by using Eq. (6) [21].

$$\frac{Ce}{qe} = \frac{Ce}{Q} + \frac{1}{Qb} \tag{5}$$

where Q (mg/g) is the maximum adsorption capacity and b (L/mg) represents Langmuir constant associated with the affinity of binding sites.

$$\log q_e = \log K_F + \frac{1}{n}\log C_e \tag{6}$$

where k_F (mg/g) and n are Freundlich constants related to adsorption capacity and adsorption intensity, respectively.

2.4.5. Desorption study

The adsorption was done using 10 mL of 50 mg/L rotenone solution with 10 mg of each CS-GO nanocomposite at 25 °C for 60 min. The solution was then filtered and the CS-GO nanocomposites were collected and dried. The desorption study was carried out by immersing the rotenone-loaded CS-GO nanocomposite in 10 mL of 0.25 mol/L HCl or NaOH aqueous solution at 25 °C for 60 min. The CS-GO was then removed from the solution. The amount of rotenone desorbed from CS-GO was determined by using UV–Visible spectrophotometer. In this study, both 0.25 mol/L HCl and NaOH blanks were used as controls. Percentage of desorption was calculated by using Eq. (7) [22].

$$Desorption\ (\%) = \left(\frac{Desorbed\ [rotenone]}{Adsorbed\ [rotenone]}\right) \times 100 \tag{7}$$

3. Results and discussion

3.1. Characterisation study

3.1.1. FTIR spectroscopy analysis

Fig. 1 shows FTIR spectra of GO, CS and CS-GO nanocomposite. Fig. 1a presents major absorption bands of GO in the FTIR spectrum appearing at 3372, 3000 1737, 1645, 1317, 1155 and 1086 cm^{-1}. The absorption band observed at 3372 cm^{-1} represents OH groups, while the band at 3000 cm^{-1} corresponds to C—H stretch of GO [16]. FTIR spectrum of GO exhibits two typical peaks at 1737 and 1645 cm^{-1} which can be assigned to vibration stretching of C═O of COOH groups and C═C stretching mode of the sp^2 carbon skeletal network or epoxy groups, respectively [23]. In addition, the absorption peaks appeared at 1317, 1155 and 1086 cm^{-1} can be related to C—O vibration of various oxygen-containing groups such as epoxy and carboxyl groups [24]. These groups favour the miscibility and dispersion of GO in polymer matrix via hydrogen bonding or electrostatic interactions [25].

The FTIR spectrum of CS (Fig. 1b) exhibits several distinctive absorption bands. A broad absorption band observed at 3367 cm^{-1} can be attributed to the stretching vibration of OH groups which is overlapped with N—H stretching vibration. The asymmetric stretching vibrations of aliphatic C—H of CS stretch were represented by absorption bands at wavenumbers of 2927 and 2925 cm^{-1}. An absorption band appeared at 1647 cm^{-1} represents amide I, while the peak at 1559 cm^{-1} ascribed amide II [26]. Meanwhile, another peaks observed at 1121 and 1072 cm^{-1} could be due to contribution of the three distinct vibration modes of C—O stretch of primary alcoholic group (CH_2-OH), C-O-C and C—C ring vibrations [27].

As can be seen from Fig. 1c, the FTIR spectrum of CS-GO nanocomposite presents a combination of CS and GO characteristics (Fig. 1a and b). From Fig. 1c, it is apparent that incorporation of GO and CS has resulted in several changes to FTIR spectrum of CS-GO nanocomposite. For example, the COOH peak of GO at 1737 cm^{-1} and NH_2 peak of CS at 1559 cm^{-1} have disappeared. Meanwhile, a new absorption band was observed at 1665 cm^{-1}, which corresponds to amides (C═O stretching vibrations of –NHCO). This observation can be related to reaction of carboxyl groups of GO with amino groups of CS. This finding corroborates the disappearance of both COOH and NH_2 groups as mentioned earlier. A new band appeared at 1552 cm^{-1} could be attributed to amide II groups formed due to reaction between amino groups of CS and epoxy groups of GO. Meanwhile, a discernible peak at 1480 cm^{-1} can be ascribed as stretching vibration of carboxylate groups (-O-C═O) [16]. The shift in wavenumber of hydroxyl groups from 3372 to 3399 cm^{-1} might be due to formation of hydrogen bonding during interaction of GO and CS.

3.1.2. CHNO elemental analysis

As shown in the Table 1, the GO contains 72.73% of C and 25.78% of O. Meanwhile, CS contains 44.08% of C and 41.06% of O. The C/O ratios for GO and CS were determined as 2.82 and 1.07, which almost similar value as reported by Ferreira et al. [28] and Sessarego et al. [29], was up to ~2.0 and 1.094, respectively. Meanwhile, the C/O ratios for CS-GO 1% (w/w), CS-GO 2% (w/w) and CS-GO 3% (w/w) were 2.83, 2.73 and 2.79, respectively. Based on these values, the CS-GO nanocomposites exhibited a similar C/O ratio value of GO (2.82), as discussed earlier. The results indicate that the CS-GO nanocomposites mimic GO behaviour in terms of polarity and number of oxygen-containing groups.

The higher value of H composition led to the higher value of H/C ratio, which indicated less aliphatic properties of the compound. Commonly, both aliphatic compounds and carbohydrate have an H/C ratio

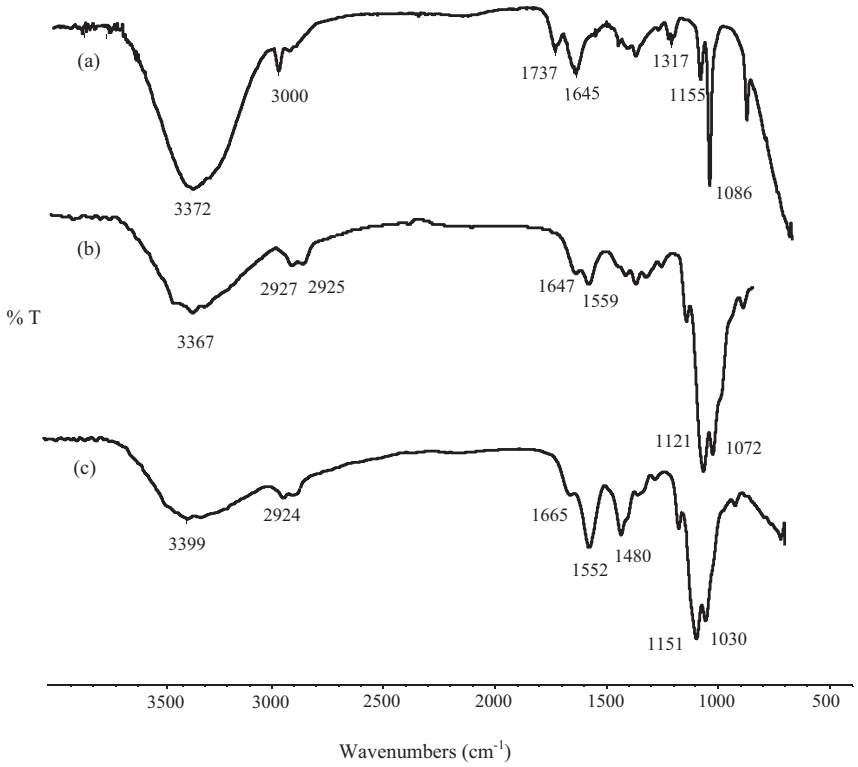

Fig. 1. FTIR spectra of (a) GO, (b) CS and (c) CS-GO 3% (w/w).

between 1.5 and 2.0, and phenolic compounds have less than 1.5 [30]. In this experiment, H/C ratio for CS and GO was determined as 0.18 and 0.02, respectively. Meanwhile, the H/C ratios for CS-GO 1% (w/w), CS-GO 2% (w/w) and CS-GO 3% (w/w) were 0.08, 0.03 and 0.02, respectively. The introduction of GO into CS, has drastically reduced the H/C ratio of CS and thus, increased the aliphatic properties of the nanocomposites.

From Table 1, it is clear that an increase in the loading level of GO from 1% (w/w) to 3% (w/w) has increased the weight percent of C and O in CS-GO nanocomposite. For example, the weight percent of C increased from 66.75% to 71.03%, when the GO loading level was increased from 1% to 3% (w/w). Meanwhile, the O content was increased from 23.56% to 25.37% following addition of GO from 1% to 3% (w/w). The higher content of oxygen-containing functional groups may provide more reactive sites for further surface or chemical interactions. On the other hand, N content showed an important loss in CS-GO nanocomposite (1.83 to 4.87%) when comparing to CS (6.92%). This probably due to increment in number of carboxyl group in GO reacts with amino group of CS to form amides. Overall, the experimental values of C, H, N and O determined in CS, GO and CS-GO nanocomposites were close to their theoretical values, presented in bracket. Hence, these findings suggest the CS-GO nanocomposites were successfully synthesised.

3.1.3. SEM analysis

CS displays a smooth, dense, uniform and some grooves texture, as shown in Fig. 2a. Meanwhile, pure GO exhibits a sheet-like structure with a wrinkled and curled surface morphology (Fig. 2b). The wrinkles and pleats are often observed for GO and graphene. These characteristics are important to maintain a high surface area and prevent collapse back into a graphitic structure [31]. Unlike pure CS, the surface of CS-GO 1% (w/w), CS-GO 2% (w/w) and CS-GO 3% (w/w) nanocomposites (Fig. 2c, d and e) became coarse and exhibited a small cluster of particles attributed to the presence of GO. The extent of roughness and clusters of particles increased with the increase in GO loading from 1% (w/w) to 3% (w/w). The presence of bright spherical structures indicates even distribution of GO nanosheets in clouded structure of CS. A similar observation of formation of small aggregates was reported by Li et al. [32], when cyclodextrin and chitosan were added to reduced GO (rGO).

Based on SEM analysis, it is clear that the increment in GO loading level, will increase the appearance of GO sheets on the surface of CS. A pronounce effect was obtained for CS-GO 3% (w/w), whereby the morphology of CS-GO 3% (w/w) shows a dense accumulation of GO dispersion. The addition of GO into polymer matrix might improve the surface area, which potentially enhance the adsorption site. This scenario provides advantageous condition for attracting more target substances

Table 1
Elemental composition of GO, CS-GO 1% (w/w), CS-GO 2% (w/w) and CS-GO 3% (w/w).

Sample	Chemical formula	Molecular weight (g/mol)	Weight percent (%)					
			C	H	N	O	C/O ratio	H/C ratio
GO	$(C_{138}H_{50}O_{21})_n$	2043.86	72.73 ± 0.6 (72.14)	1.49 ± 1.2 (1.65)	–	25.78 ± 0.4 (26.21)	2.82	0.02
CS	$(C_7H_{15}NO_4)_n$	177.20	44.08 ± 0.2 (45.65)	7.94 ± 0.8 (7.66)	6.92 ± 0.1 (7.60)	41.06 ± 0.5 (39.09)	1.07	0.18
CS-GO 1% (w/w)	$(C_{154}H_{81}N_3O_{47})_n$	2725.28	66.75 ± 0.2 (66.59)	5.84 ± 0.4 (5.99)	3.85 ± 0.6 (4.53)	23.56 ± 0.3 (22.89)	2.83	0.08
CS-GO 2% (w/w)	$(C_{287}H_{115}N_3O_{86})_n$	4980.95	67.94 ± 1.2 (68.23)	2.39 ± 0.7 (2.52)	4.87 ± 0.9 (4.66)	24.80 ± 1.1 (24.59)	2.73	0.03
CS-GO 3% (w/w)	$(C_{418}H_{143}N_3O_{122})_n$	7158.55	71.03 ± 0.8 (70.45)	1.77 ± 0.2 (1.69)	1.83 ± 0.5 (1.56)	25.37 ± 0.7 (26.30)	2.79	0.02

Theoretical values are in brackets. Values represent mean of three replicates ± standard deviation.

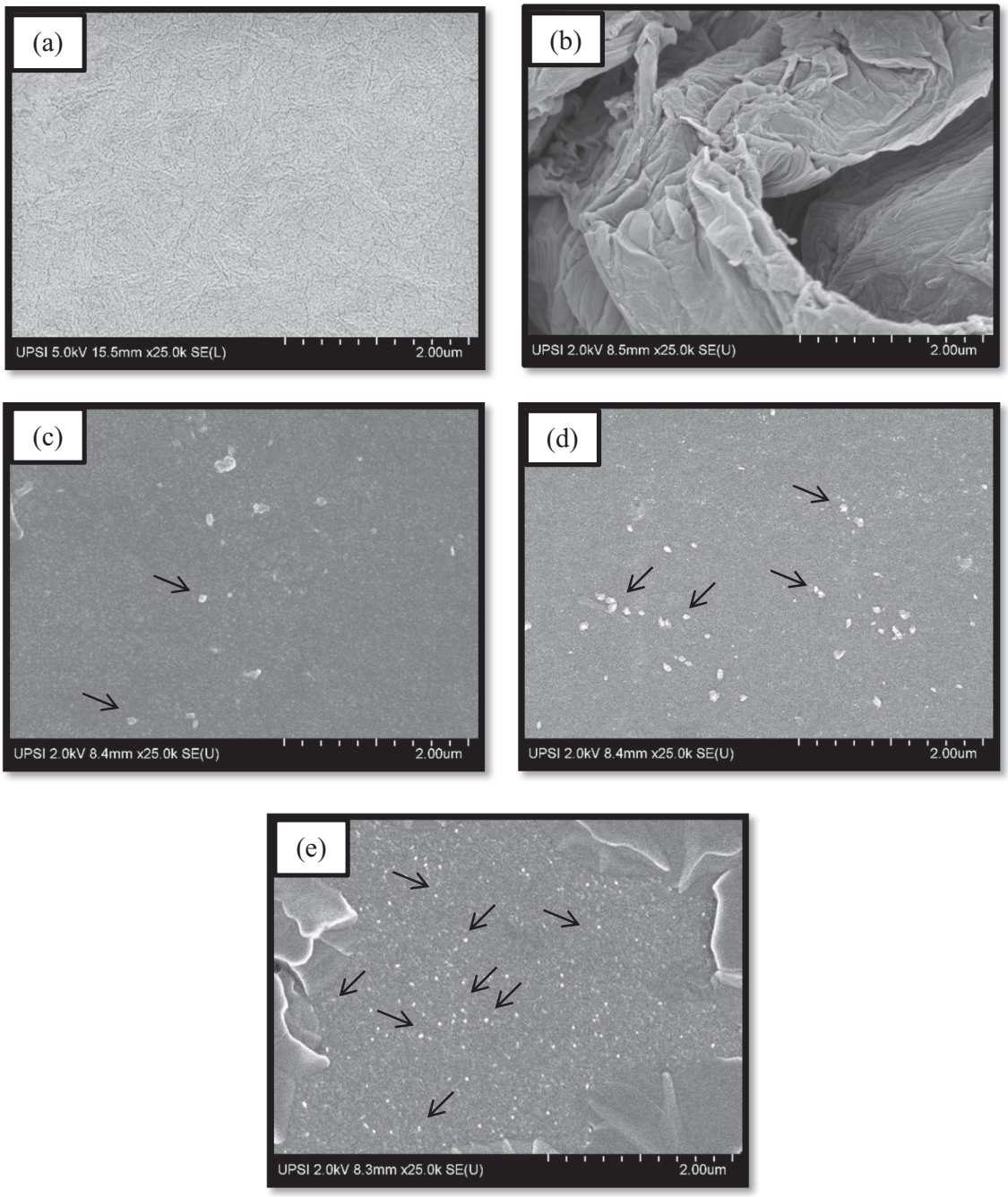

Fig. 2. SEM images of (a) CS, (b) GO, (c) CS-GO 1% (w/w), (d) CS-GO 2% (w/w) and (e) CS-GO 3% (w/w) at 25,000× magnification.

around the sites, which will greatly improve the adsorption rates of substances.

3.1.4. TEM analysis

In this study, the size of GO nanoparticle aggregates was also determined and observed at 200,000× magnification (Fig. 3). As shown in Fig. 3a, pure GO illustrates spherical-shape of nanoparticles with the size between 25.8 and 57.5 nm. For CS-GO 1% (w/w), the size for GO aggregates ranged from 23.8 to 28.8 nm (Fig. 3b). Meanwhile, CS-GO 2% (w/w) exhibited GO aggregates in the range of 18.8 to 34.7 nm (Fig. 3c). The most abundant content of GO nanoparticles can be seen for CS-GO 3% (w/w) (Fig. 3d), with the size ranged from 1.4 to 21.8 nm. It is apparent that following interaction with CS, there was a marginal decrease in size of GO nanoparticles. Previously, Khawaja et al. [33] reported that the TEM image of GO exhibited spherical-shape of nanoparticles with diameter ranging from 15 to 25 nm.

The nanoparticle size distribution plays an important role in immobilising and affects the loading capacity and binding ability of composite for active compounds [34]. Nanocarrier size is among the most important parameters in a delivery system because it can influence in vivo distribution, toxicity, targeting, loading, release, and in vitro and in vivo stability [35]. In this context, it can be speculated that CS-GO nanocomposites could be effective as hydrophilic sites for hydrophobic rotenone in adsorption system.

3.1.5. XRD analysis

Fig. 4 shows X-ray diffractograms of GO, CS and CS-GO nanocomposites. The X-ray diffractogram of GO (Fig. 4a) exhibits a very intense peak at $2\theta = 10.5°$ (about 20,000 counts), which corresponds to a d-spacing

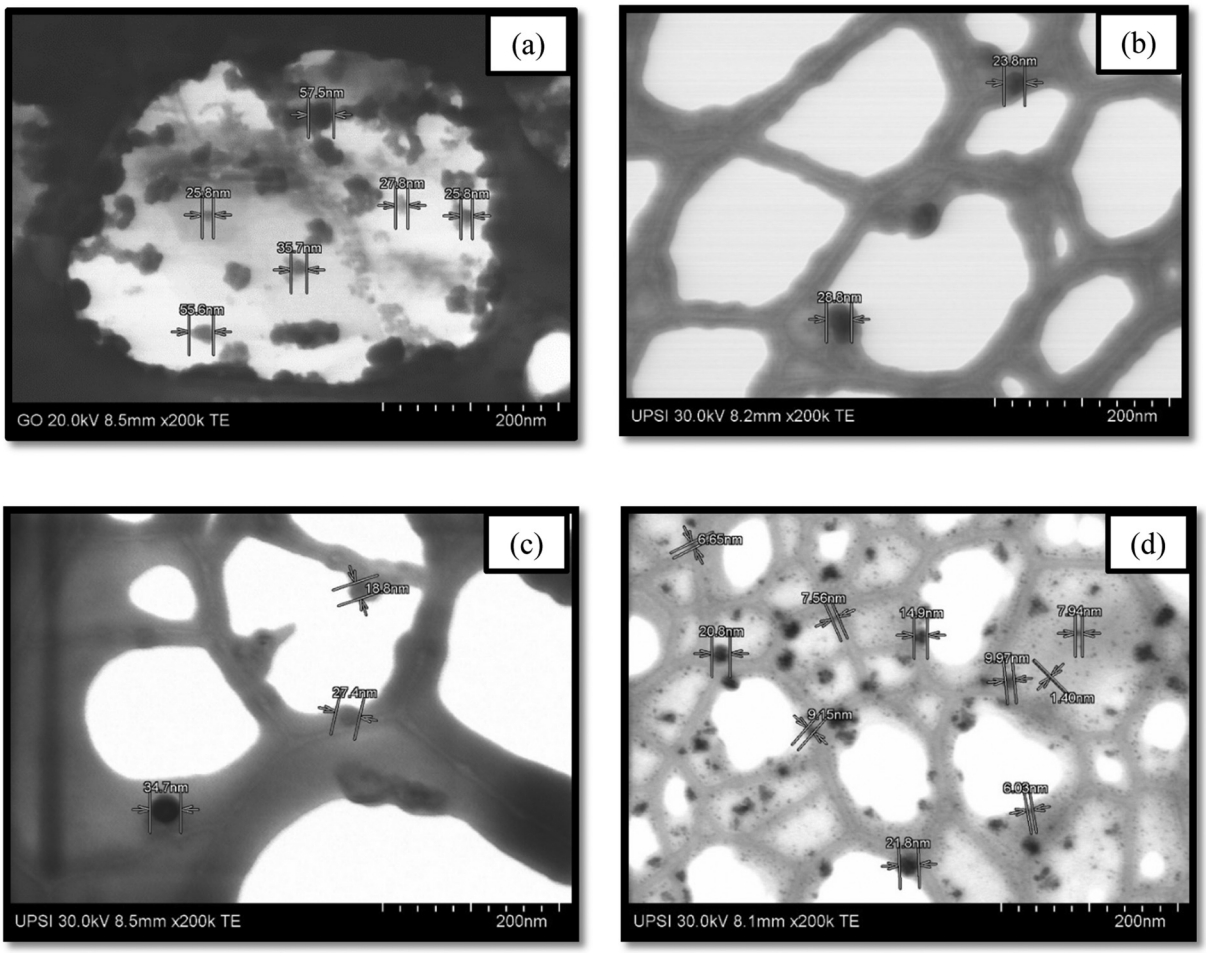

Fig. 3. TEM images of (a) GO, (b) CS-GO 1% (w/w), (c) CS-GO 2% (w/w) and (d) CS-GO 3% (w/w) at 200,000× magnification.

of 7.91 nm as estimated by Bragg's law [36]. It can also be related to the large amount of polar functional groups generated between graphene layers during oxidation [37]. Meanwhile, X-ray diffractograms of CS (Fig. 4b) were observed at $2\theta = 10.8°$, 16.5° and 20.42°. Of these three structural peaks for CS, the peak at $2\theta = 20.42°$ was the most prominent with a signal counts value of about 3000.

As depicted in Fig. 4c, d and e, there is no structural peak represents GO in CS-GO nanocomposites. The main diffractive regions of CS-GO nanocomposites were observed at $2\theta = 16.5°$ and 20.42°. These peaks represent diffractive characteristics for CS, which have been mentioned earlier for X-ray diffractogram of CS (Fig. 4b). The disappearance of GO peak suggests that most of the GO reacted with CS. Amines of the CS reacted with carbonyl and epoxyl group of GO, thus might have an effect to the layered structure and crystallinity property [37]. It is apparent that the intensity of diffractive peak at $2\theta = 20.42°$ of CS increased from 3000 counts (Fig. 4b) to more than 4000 counts (Fig. 4c, d and e). The peak intensity were correlated with the degree of crystalline region. Hence, it is interesting to note that the addition of GO into CS, increased the crystallinity degree of CS.

Overall, results from XRD analysis highlights the marginal increment in diffractive peak of CS at $2\theta = 20.42°$ following addition of GO into CS. This increment might have an effect on adsorption capacity of CS-GO nanocomposites for rotenone.

3.2. Performance study

3.2.1. Solubility study

The solubility study of CS, CS-GO 1% (w/w), CS-GO 2% (w/w) and CS-GO 3% was conducted to evaluate the pH dependence of the water solubility of each nanocomposite. In this study, the ability of each nanocomposite was tested at solution pH ranged from 1 to 13. The solubility was measured as percentage of transmittance of UV–Visible which passed through the nanocomposites solutions. The water solubility of nanocomposites are depicted in Fig. 5.

From Fig. 5, the transmittance of both CS and CS-GO nanocomposites solutions were close to 100% at low pH (pH ≤ 6.0), indicating that the compounds were all soluble in water in this pH range. The optical transmittance of the CS solution dropped sharply from its initial level at pH ≤ 6 (98.30% to 99.56%) down to almost insoluble levels (18.29% to 35.07%) at pH ≥ 7 and the solution became opaque. In contrast, the transmittance of CS-GO nanocomposites declined by a small extent with percentage of reduction between 18.65% and 32.71%.

CS is typically water-soluble in acidic medium due to protonation of the amino groups (NH_3^+) [38]. As discussed by Rui et al. [39] CS can be partially hydrolysed to achieve water solubility by obtaining shorter chain lengths with more free amino groups in D-glucosamine units as a result of a decrease in molecular weight. However, CS has low solubility at neutral and alkaline conditions. Alternatively, the destruction of intermolecular and intramolecular hydrogen bonds is favourable to the reduction of CS crystallinity and improvement of its solubility [40].

The water solubility of CS-GO nanocomposites increased with increasing of GO loading levels. The transmittance percentages of CS-GO 1% (w/w), CS-GO 2% (w/w) and CS-GO 3% (w/w) were increased more than 60% at pH range of 7 to 13. In this pH range, CS-GO 3% (w/w) exhibited the highest solubility in water with transmittance percentage of 80.67% to 86.58%, followed by CS-GO 2% (w/w) (70.08% to 75.01%) and CS-GO 1% (w/w) (63.07% to 68.21%). This observation indicates that the introduction of GO to CS backbone improved the solubility

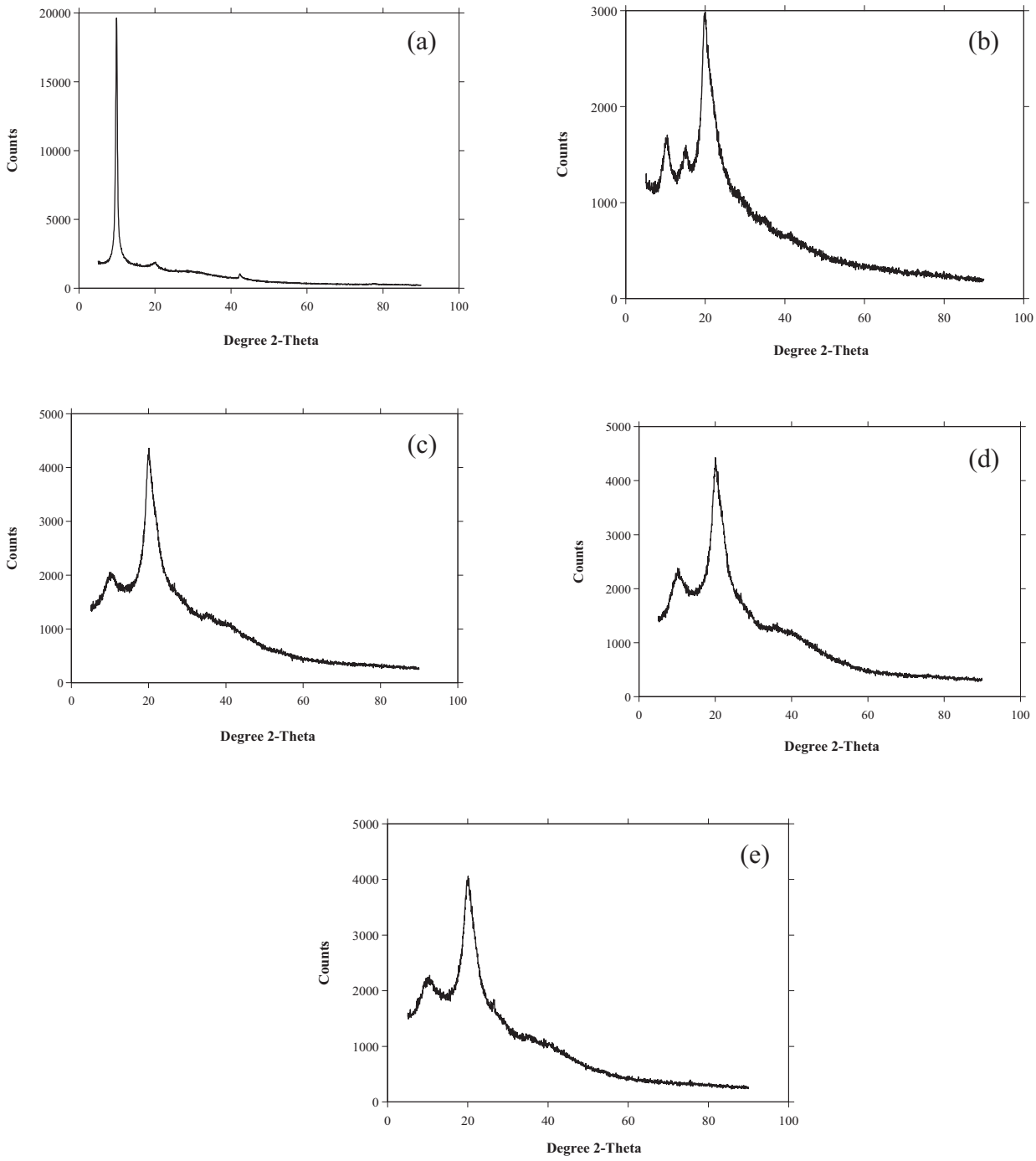

Fig. 4. XRD patterns of (a) GO, (b) CS, (c) CS-GO 1% (w/w), (d) CS-GO 2% (w/w) and (e) CS-GO 3% (w/w).

of CS over the entire pH values studied. Furthermore, the addition of GO could have an effect in damaging the regularity of chitosan chain and the structure of hydrogen bonds, leading to a significant increment in hydrophilicity of the copolymers [23,41]. As discussed by Chen et al. [42] the hydrophilic pendant hydroxyl groups on GO could form hydrogen bonds with amino and hydroxyl groups of CS, and broke the intra/intermolecular hydrogen bonds of CS. This phenomenon significantly improved the water solubility of CS-GO.

3.2.2. Adsorption study

3.2.2.1. Effect of solution pH. The effect of solution pH on adsorption of rotenone by CS-GO nanocomposites are presented in Fig. 6a. All nanocomposites show a similar trend in rotenone uptake, whereby the capacity decreased when the solution pH was increased. Adsorption capacity of CS-GO nanocomposites towards rotenone displayed a marked decrement in basic media (pH 8 and 9). A pronounce effect was observed at pH 9, of which the adsorption capacities of CS-GO nanocomposites drastically increased (0.73 to 10.8 mg/g) with the increment of GO loading in nanocomposites from 1% to 3% (w/w). The influenced of GO loaded on the adsorption capacity of nanocomposites can be clearly seen at pH 1, whereby the highest adsorption capacity was exhibited by CS-GO 3%. The increment of GO loading levels has increased the oxygen-containing groups of the nanocomposites, thus enhances the hydrogen-bonding sites for rotenone. The overall results suggest that the interaction of rotenone and CS-GO nanocomposites was favourable in acidic media.

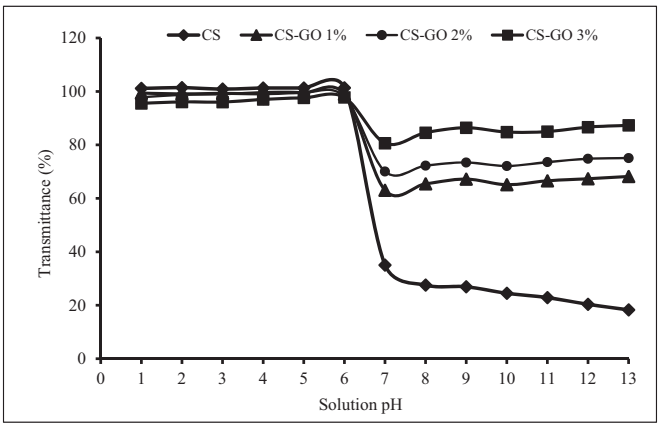

Fig. 5. Water solubility of CS, CS-GO 1% (w/w), CS-GO 2% (w/w) and CS-GO 3% (w/w) as a function of pH.

According to Fig. 7, the main mechanism for rotenone adsorption is believed to be through hydrogen bonding and π-π interaction. Since CS-GO has both –OH and –COOH groups, these functional groups or residual oxygen-containing groups of GO can form hydrogen bond with rotenone. The second mechanism could be attributed to the contribution of GO through the π-π interaction between aromatic ring of GO and rotenone as hydrophobic compound.

The -NHCO- groups in CS-GO nanocomposite became protonated (Fig. 7a). The protonation of this amide surface group has provided more hydrogen bonding sites to increase the capacity of rotenone adsorption. In addition, hydrophobic groups of rotenone are also attracted by the benzene ring due to the hydrophobic effect and π-π bonds interaction. Fig. 7b shows the proposed mechanism for rotenone adsorption in acidic medium. In the acidic background, the high concentration of H^+ ion has led the –OH and –COOH groups of CS-GO nanocomposites remained in the form of –OH and –COOH. Therefore, the formation of hydrogen bonding between –OH and –COOH in nanocomposites and rotenone is favourable.

However, a different reaction occurred as the solution pH was increased. Fig. 8c describes the proposed mechanism of rotenone adsorption in basic medium. With the increasing of solution pH, less protons were available to protonate the imine groups leading to the decrease of hydrogen-bonding sites and thus reduce the adsorption capacity of CS-GO nanocomposites. On the other hand, the increment of pH value had encouraged the formation of COO^- (Fig. 8a), which against the formation of hydrogen bonds and also leading to the decrease of adsorption capacity. In addition, the dissociation of –OH group of phenol (Fig. 8b) had increased hydrophilicity of the nanocomposites that may lead to the decrease in hydrophobic interaction and hydrogen bond formation with rotenone.

The proposed mechanism of CS-GO interaction with rotenone was further supported by FTIR analysis. Fig. 9 shows FTIR spectra of CS-GO before and after interaction with rotenone. FTIR spectrum of CS-GO nanocomposite (Fig. 9a) apparently changed and showed several distinctive characteristics following adsorption of rotenone (Fig. 9b). The wavenumber of absorption band at 3399 cm^{-1} was shifted to 3238 cm^{-1} and its absorption intensity reduced significantly, confirming the involvement of hydroxyl groups of CS-GO nanocomposites in binding rotenone molecules by formation of hydrogen bonding. A similar trend of change can be observed for the band at 1576 cm^{-1} which resulted from the formation of hydrogen bond between secondary amine group of CS-GO with rotenone. A part from that, the peak at 1409 cm^{-1} has vanished and a new flatten peak appeared at 1419 cm^{-1}, which indicates the interaction of CS-GO with rotenone has occurred.

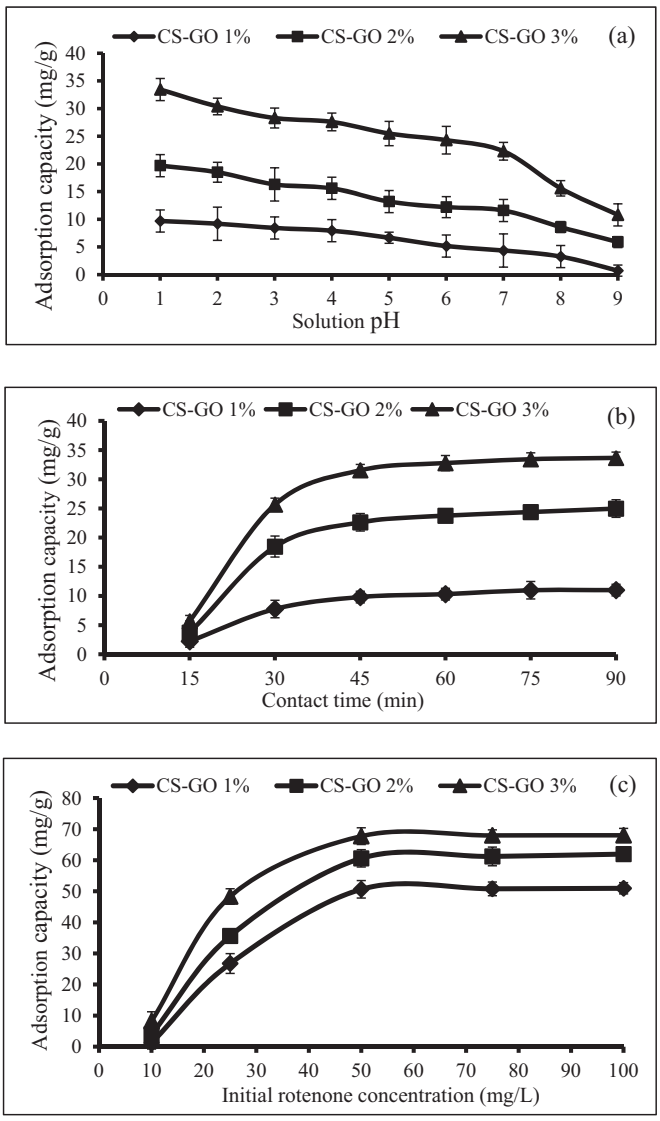

Fig. 6. Adsorption of rotenone onto CS-GO nanocomposites as influenced by (a) effect of solution pH, (b) effect of contact time (min) and (c) effect of initial rotenone concentration (mg/L).

3.2.2.2. Effect of contact time. In addition to solution pH, the adsorption capacity of CS-GO 1% (w/w), CS-GO 2% (w/w) and CS-GO 3% (w/w) for rotenone was also studied as a function of contact time as shown in Fig. 6b. From Fig. 6b, the adsorption capacities of the nanocomposites were relatively rapid at the first 30 min of the experiment before the equilibrium was reached at 90 min. At the first 30 min, the adsorption capacity of CS-GO 1% (w/w) reached to 7.77 mg/g followed by the CS-GO 2% (w/w) and CS-GO 3% (w/w) which are 18.47 mg/g and 25.67 mg/g, respectively. The fast adsorption rate at the initial stage can be related to the presence of large number of vacant sites in which rotenone molecule can easily interact with these sites. As the GO loading levels increase from 1% (w/w) to 3% (w/w), the number of vacant sites have also increased.

Once equilibrium has been attained, the active sites of CS-GO nanocomposites are filled with rotenone. At optimum contact time (90 min), the adsorption capacities of CS-GO nanocomposites were 33.67 mg/g (CS-GO 3% (w/w)), 24.99 mg/g (CS-GO 2% (w/w)) and 11.01 mg/g (CS-GO 1% (w/w)), respectively. From Fig. 6b, it is apparent that there was no significant difference in terms of adsorption capacities determined at contact time of 75 and 90 min. For example, the adsorption capacities of CS-GO 3% (w/w) at 75 and 90 min were 33.45 and 33.67 mg/

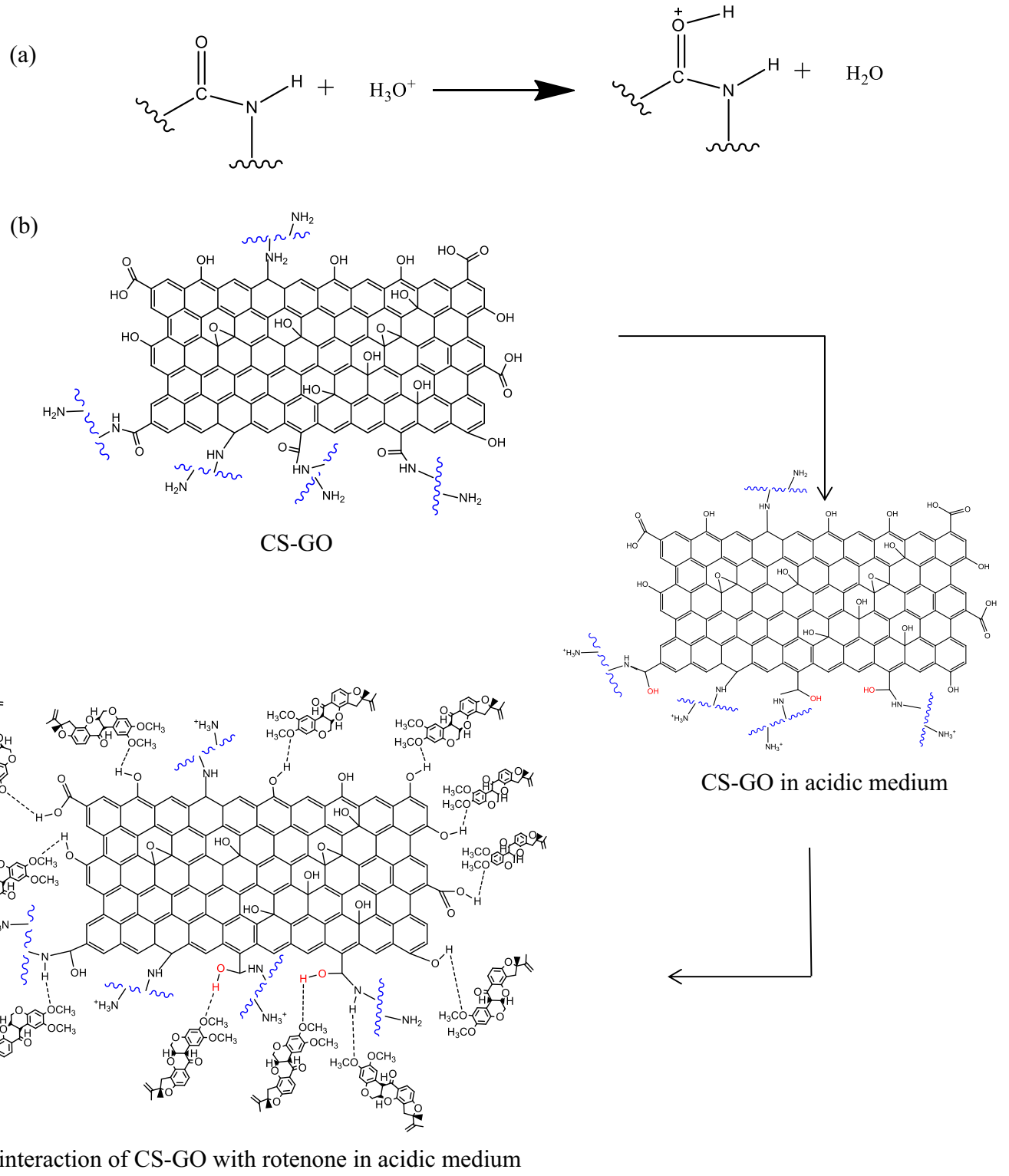

Fig. 7. (a) Reaction scheme of imine groups in acidic medium and (b) mechanism of CS-GO interaction with rotenone in acidic medium.

g, respectively. This phenomenon can be related to the repulsion forces between rotenone molecules on CS-GO nanocomposites and bulk phase, which it caused the adsorption capacity to reach equilibrium.

3.2.2.3. Effect of initial concentration. As shown in Fig. 6c, CS-GO 1% (w/w), CS-GO 2% (w/w) and CS-GO 3% (w/w) nanocomposites have demonstrated a significant rapid increment in adsorption capacity when initial concentration was increased from 10 to 30 mg/L. For example, the adsorption capacity of CS-GO 3% (w/w) for rotenone was increased from 8.23 mg/g to 48.33 mg/g, which represent an 82.97% increment. This rapid increment at such concentration was probably due to the increase in number of rotenone molecules available to be adsorbed at the vacant sites of nanocomposites.

CS-GO 1% (w/w), CS-GO 2% (w/w) and CS-GO 3% (w/w) showed a similar trend in adsorption capacity, of which as the initial rotenone concentration increased the adsorption capacity increased

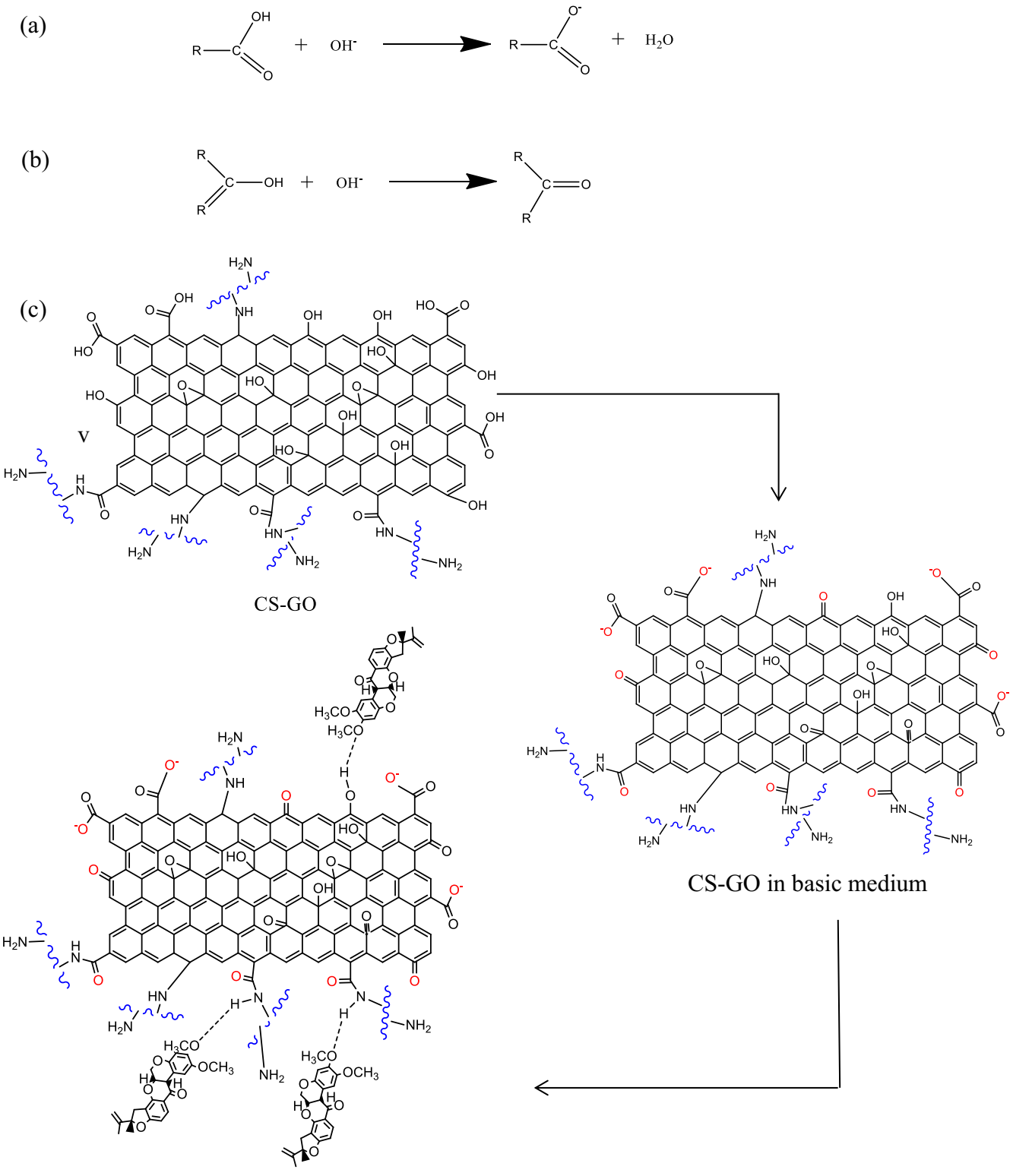

Fig. 8. (a) Reaction scheme of carboxyl groups in basic medium, (b) reaction scheme of hydroxyl groups in basic medium and (c) mechanism of CS-GO interaction with rotenone in basic medium.

until it attained the equilibrium state. The number of active sites on the CS-GO nanocomposites was constant, but the number of rotenone molecules increased as the concentration of rotenone increased. However, the saturation of CS-GO nanocomposites surface at high concentration of rotenone molecules has been a major cause of the equilibrium process. On the other hand, at high concentrations, more amount of rotenone molecules unadsorbed in a certain volume of solutions and thus adsorption capacity remains unchanged. Based on results obtained, 50 mg/L was chosen to be the optimum initial concentration.

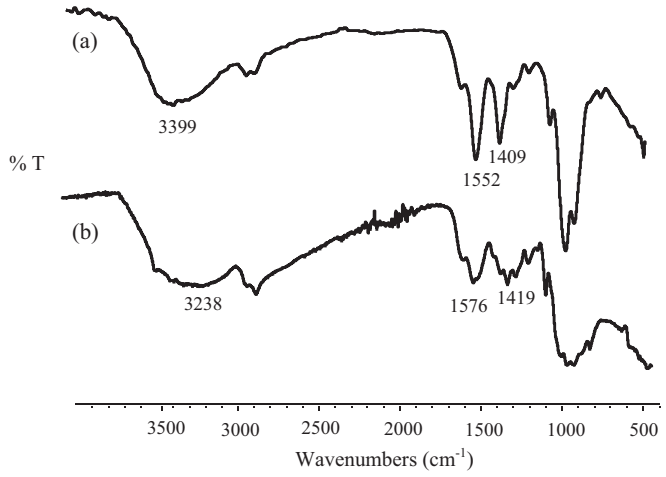

Fig. 9. FTIR spectra of (a) CS-GO before interaction with rotenone and (b) CS-GO after interaction with rotenone.

3.3. Adsorption kinetic study

In this study, the adsorption kinetic data were fitted to pseudo-first order, pseudo-second order and intraparticle diffusion kinetic equations in order to determine the adsorption rate and controlling mechanism of the adsorption process. Pseudo-first order suggests that the rate of adsorption is dependant on the difference between the q_e and the q_t, which relates to the driving force for mass transfer of adsorbate to reach the surface of adsorbent [43]. Meanwhile, pseudo-second order model is based on the assumption that the rate-limiting step may be chemical sorption [44]. Intraparticle diffusion model explains that the adsorption of adsorbates is controlled by the diffusion process, namely pore diffusion or intraparticle diffusion [45].

Table 2 lists the parameters of pseudo-first order, pseudo-second order and intraparticle diffusion kinetic models for adsorption of rotenone onto CS-GO nanocomposites. Based on correlation coefficient (R^2), the kinetic data followed the pseudo-first order kinetic model and surface physical adsorption might be the rate-limiting step for rotenone adsorption by CS-GO nanocomposites. The R^2 values for rotenone adsorption by CS-GO 1% (w/w), CS-GO 2% (w/w) and CS-GO 3% (w/w) were determined as 0.9897, 0.9909 and 0.9947, respectively. As the GO loading level was increased from 1% to 3% (w/w), the adsorption-vacant site of CS-GO nanocomposites was also increased. Hence, the adsorption of rotenone onto CS-GO 1% (w/w) was more rapid to reach equilibrium (0.069 min^{-1}) as compared to CS-GO 3% (w/w) (0.183 min^{-1}). This could be the reason for k_1 (min^{-1}) values increased with increasing of GO loading levels.

3.4. Adsorption isotherm study

In this study, the Langmuir and Freundlich isotherm models with their constant values, which describe the surface properties and affinity of the adsorbent, have been used to understand the mechanism of adsorption. The Langmuir model was based on the assumption that there are energetically equivalent numbers of adsorption sites on the adsorbent surface. The binding of adsorbates to the adsorption sites can be classified either chemical or physical, but it must be sufficiently effective to prevent displacement of the adsorbates on neighbouring sites [46]. Meanwhile, Freundlich model predicts multilayer adsorption on a heterogeneous adsorption surface with unequal available sites with different adsorption energies [47].

Table 3
Parameters of Langmuir and Freundlich isotherm models for adsorption of rotenone onto CS-GO nanocomposites.

Adsorbent	Langmuir			Freundlich		
	Q (mg/g)	b (L/mg)	R^2	K_F (mg/g)	n	R^2
CS-GO 1% (w/w)	69.93	0.0314	0.9989	2.1134×10^{-3}	0.6400	0.8106
CS-GO 2% (w/w)	77.51	0.0852	0.9879	0.1523	0.8582	0.8287
CS-GO 3% (w/w)	92.59	0.0285	0.9956	2.9228	1.1252	0.8030

The parameters of Langmuir and Freundlich isotherm models for adsorption of rotenone onto CS-GO nanocomposites are given in Table 3. The results show that the equilibrium isothermal data of CS-GO 1% (w/w), CS-GO 2% (w/w) and CS-GO 3% (w/w) were perfectly fitted to the Langmuir model with R^2 values of 0.9989, 0.9879 and 0.9956, respectively. Based on Table 3, the maximum adsorption capacity (Q) for CS-GO 1% (w/w), CS-GO 2% (w/w) and CS-GO 3% (w/w) were 69.93 mg/g, 77.51 mg/g and 92.59 mg/g, respectively. Interestingly, the adsorption capacity of CS-GO for rotenone was correlated well with the GO content. A similar trend was observed by the Qi et al. [46]. In their study, the Q of methylene blue onto GO/CS sponge was reported to increase when the GO content of GO/CS sponge was increased from 45% to 97%. The Q was reported as 275.5 mg/g for GO/CS (CS content 9%; GO content 91%).

It is thus reasonable to infer that adsorption of rotenone by CS-GO nanocomposites was mainly attributed to GO. In this context, the maximum adsorption capacity greatly determines the ability of CS-GO nanocomposites to dissolve rotenone in certain volume of water. For instance, the CS-GO 3% (w/w) was able to increase the solubility of rotenone by 46.30% when it adsorb 92.59 mg of rotenone in 1 L of water. Overall, the CS-GO 1% (w/w), CS-GO 2% (w/w) and CS-GO 3% (w/w) increased the solubility of rotenone in water by 34.40%, 38.80% and 46.30%, respectively.

3.5. Desorption study

The adsorption and desorption capacities are the two key criteria in evaluating the applicability of a material to be used as a carrier agent for hydrophobic compounds. An ideal material for carrier system should not only possess high adsorption capacity but should also be able to withstand at such acidic and basic media. Materials with high desorption percentage at certain media are normally not favourable to be used in carrier system. Desorption is an interfacial process affecting the mobility and fate of adsorbates in water environments [29]. In this context, studying desorption behaviour will give insight into the reversibility of CS-GO and rotenone interactions. In this study, adsorption–desorption cycles of rotenone were repeated three times in order to evaluate the reusability of the nanocomposites.

Table 2
Parameters of pseudo-first order, pseudo-second order and intraparticle diffusion kinetic models for adsorption of rotenone onto CS-GO nanocomposites.

Adsorbent	Pseudo-first order model			Pseudo-second order model			Intraparticle diffusion model	
	k_1 (min^{-1})	q_e (mg/g)	R^2	k_2 (g mg^{-1}/ min)	q_e (mg/g)	R^2	k_{id} (mg/ g $min^{-0.5}$)	R^2
CS-GO 1% (w/w)	0.069	12.99	0.9897	2.69×10^{-5}	86.20	0.0482	0.1237	0.8484
CS-GO 2% (w/w)	0.099	25.97	0.9909	1.48×10^{-5}	151.51	0.0286	0.2478	0.7052
CS-GO 3% (w/w)	0.183	33.67	0.9947	1.90×10^{-7}	166.67	0.0019	0.3114	0.6283

Temperature, 25 °C; initial rotenone concentration, 50 mg/L; mass of adsorbent, 10 mg; volume of solution, 10 mL; pH of the solution, 1.0.

Table 4
Desorption percentage of rotenone from CS-GO nanocomposite in acidic and basic condition.

Adsorbent	Desorption (%)					
	HCl			NaOH		
	First cycle	Second cycle	Third cycle	First cycle	Second cycle	Third cycle
CS-GO 1% (w/w)	60.14	53.92	38.37	94.57	89.21	85.78
CS-GO 2% (w/w)	51.53	45.86	36.39	83.42	79.60	74.46
CS-GO 3% (w/w)	32.86	26.45	16.64	78.86	73.83	69.41

The adsorption data (Section 3.2.2.1) indicated that the rotenone adsorption onto CS-GO nanocomposites was pH-responsive particularly at low pH media. Irreversibly, rotenone desorption from CS-GO nanocomposites was expected to be successful at high pH values. From Table 4, it was revealed that the desorption performance of rotenone with 0.25 mol/L of HCl was found to be rather low, as compared to when 0.25 mol/L NaOH was used as desorption agent. For instance, it is apparent that for the first cycle of adsorption-desorption 94.57%, 83.42% and 78.86% of rotenone was desorbed from CS-GO 1% (w/w), CS-GO 2% (w/w) and CS-GO 3% (w/w) in 0.25 mol/L NaOH solution, respectively. It is interesting to note that although HCl and NaOH have different desorption capacity, the trend in desorbing rotenone from CS-GO nanocomposites was similar, in the order of CS-GO 1% (w/w) > CS-GO 2% (w/w) > CS-GO 3% (w/w). This suggests that rotenone was tightly hold by CS-GO 3% (w/w).

As shown in Table 4, it is clear that the recovery and amount of rotenone adsorbed onto CS-GO nanocomposites decreased following 3 cycles of adsorption–desorption process. The reduction in recovery of CS-GO nanocomposites was within 15.14 to 21.77% when 0.25 mol/L HCL was used as desorption agent. Meanwhile, a smaller degree of reduction (8.79 to 9.45%) was obtained with 0.25 mol/L NaOH. The decrease in adsorbent adsorption ability during the regeneration process could be due to two main factors, namely a decrease in the number of adsorption sites after each desorption step and adsorbent degradation [48].

4. Conclusion

CS-GO nanocomposites at three GO loading levels, namely 1%, 2% and 3% (w/w) were successfully prepared and characterised. CS-GO nanocomposites possess ideal characteristics as nanocarriers for hydrophobic rotenone. CS-GO nanocomposites are soluble in water and exhibit high adsorption capacities at acidic media. The solubility of rotenone in water has been increased, up to 46.30% with application of CS-GO nanocomposites. Hydrogen bonding and π-π interaction are the two major mechanisms for rotenone adsorption onto CS-GO nanocomposites and surface physical adsorption might be the rate-limiting step. CS-GO 3% (w/w) was superior in binding rotenone molecules, with the lowest desorption percentage. The application of CS-GO nanocomposites as water-solubilising agents in pesticide formulations could reduce the amount of organic solvent, producing eco-friendly pesticides for a safer environment.

CRediT authorship contribution statement

Mohd Sahli Muda: Investigation, Formal analysis, Writing - original draft. **Azlan Kamari:** Funding acquisition, Project administration, Investigation, Supervision, Writing - review & editing. **Suriani Abu Bakar:** Methodology, Investigation. **Siti Najiah Mohd Yusoff:** Formal analysis, Resources. **Is Fatimah:** Methodology, Conceptualization. **Esther Phillip:** Visualization, Formal analysis. **Shahrulnizahana Mohammad Din:** Data curation, Validation.

Declaration of competing interest

The authors declare no conflict of scientific and financial interest.

Acknowledgement

This research was funded by Ministry of Education Malaysia (FRGS 2014-0105-101-02) and Islamic Educational, Scientific and Cultural Organization (ISESCO), Kingdom of Morocco.

References

[1] M. Fawzi, B. Mfarrej, F.M. Rara, Competitive, sustainable natural pesticides, Acta Ecol. Sin. 39 (2019) 145–151.
[2] S. Waidyanatha, K. Ryan, A.L. Roe, W. Jia, M.F. Paine, S. Ferguson, C. Rider, Follow that botanical: challenges and recommendations for assessing absorption, distribution, metabolism and excretion of botanical dietary supplements, Food Chem. Toxicol. 121 (2018) 194–202.
[3] S.B. Lao, Z.X. Zhang, H.H. Xu, G.B. Jiang, Novel amphiphilic chitosan derivatives: synthesis, characterization and micellar solubilization of rotenone, Carbohydr. Polym. 82 (2010) 1136–1142.
[4] P. Sarah, D. Kamarulzaman, S. Yusup, N. Osman, N. Ha, R. Yusof, R. Talib, Effectiveness of neem based biopesticide to enhance rice (*Oryza sativa*) productivity, Sustain. Chem. Pharm. 7 (2018) 36–40.
[5] K. Chang, F. Chang, M. Chen, Developing a novel cholesterol-based nanocarrier with high transfection efficiency and serum compatibility for gene therapy, J. Formos. Med. Assoc. 118 (2019) 766–775.
[6] A.N. Meredith, B. Harper, S.L. Harper, The influence of size on the toxicity of an encapsulated pesticide: a comparison of micron- and nano-sized capsules, Environ. Int. 86 (2016) 68–74.
[7] S. Kumar, V. Deepak, M. Kumari, P.K. Dutta, Antibacterial activity of diisocyanate-modified chitosan for biomedical applications, Int. J. Biol. Macromol. 84 (2019) 349–353.
[8] A. Cernat, S.J. Györfi, M. Irimes, M. Tertiş, Click chemistry on azide-functionalized graphene oxide, Electrochem. Commun. 98 (2019) 23–27.
[9] S.M. Maliyekkal, T.S. Sreeprasad, D. Krishnan, S. Kouser, A.K. Mishra, U.V. Waghmare, T. Pradeep, Graphene: a reusable substrate for unprecedented adsorption of pesticides, Small (2012)https://doi.org/10.1002/smll.201201125.
[10] L. Ding, Y. Huang, X. Cai, S. Wang, Impact of pH, ionic strength and chitosan charge density on chitosan/casein complexation and phase behavior, Carbohydr. Polym. 208 (2019) 133–141.
[11] S. Yu, X. Xu, J. Feng, M. Liu, K. Hu, Chitosan and chitosan coating nanoparticles for the treatment of brain disease, Int. J. Pharm. 560 (2019) 282–293.
[12] G. Tang, K. Tian, X. Song, Y. Xiong, S. Min, Comparison of several supervised pattern recognition techniques for detecting additive methamidophos in rotenone preparation by near-infrared spectroscopy, Spectrochim. Acta A Mol. Biomol. Spectrosc. 121 (2014) 678–684.
[13] K. Milowska, A. Szwed, M. Mutrynowska, R. Gomez-Ramirez, F.J. de la Mata, T. Gabryelak, M. Bryszewska, Carbosilane dendrimers inhibit α-synuclein fibrillation and prevent cells from rotenone-induced damage, Int. J. Pharm. 484 (2015) 268–275.
[14] S.I. Zubairi, M.R. Sarmidi, R.A. Aziz, A study of rotenone from derris roots of varies location, plant parts and types of solvent used, Adv. Environ. Bio. 8 (2015) 445–449.
[15] A. Kamari, N.F.A. Aljafree, S.N.M. Yusoff, *N,N*-dimethylhexadecyl carboxymethyl chitosan as a potential carrier agent for rotenone, Int. J. Biol. Macromol. 88 (2016) 263–272.
[16] L. Fan, K. Wang, N. Zhao, Z. Li, Z. Shi, Z. Jin Ge, Fabrication, mechanical properties, and biocompatibility of graphene-reinforced chitosan composites, Biomacromolecules 11 (2010) 2345–2351.
[17] S. Lagergren, Zur theorie der sogenannten adsorption gelöster stoffe, K. Sven. Vetenskapsakad. Handl. 24 (1898) 1–39.
[18] Y.S. Ho, G. McKay, The kinetics of sorption of divalent metal ions onto Sphagnum moss peat, Water Res. 34 (2000) 735–742.
[19] W.J. Weber, J.C. Morris, Kinetics of adsorption of carbon from solution, J. Sanitary Eng. Div. 89 (1963) 31–59.
[20] I. Langmuir, The constitution and fundamental properties of solids and liquids. Part I. Solids, J. Am. Chem. Soc. 38 (1916) 2221–2295.
[21] H.M.F. Freundlich, Über die adsorption in lasungen, Z. Phys. Chem. 57 (1906) 385–470.
[22] B.S. Stromer, B. Woodbury, C.F. Williams, Tylosin sorption to diatomaceous earth described by Langmuir isotherm and Freundlich isotherm models, Chemosphere 193 (2018) 912–920.
[23] N. Salahuddin, H. El-daly, R.G. El Sharkawy, B.T. Nasr, Synthesis and efficacy of PPy/CS/GO nanocomposites for adsorption of ponceau 4R dye, Polymer 146 (2018) 291–303.

[24] X. Jing, H. Mi, B.N. Napiwocki, X. Peng, L. Turng, Mussel-inspired electroactive chitosan/graphene oxide composite hydrogel with rapid self-healing and recovery behavior for tissue engineering, Carbon 125 (2017) 557–570.
[25] M.A. Kamal, S. Bibi, S.W. Bokhari, A.H. Siddique, T. Yasin, Synthesis and adsorptive characteristics of novel chitosan/graphene oxide nanocomposite for dye uptake, React. Funct. Polym. 110 (2017) 21–29.
[26] E.M. Fayyad, K.K. Sadasivuni, D. Ponnamma, M.A.A. Al-Maadeed, Oleic acid-grafted chitosan/graphene oxide composite coating for corrosion protection of carbon steel, Carbohydr. Polym. 151 (2016) 871–878.
[27] J. Zhang, N. Chen, M. Li, C. Feng, Synthesis and environmental application of zirconium–chitosan/graphene oxide membrane, J. Taiwan Inst. Chem. Eng. 77 (2017) 106–112.
[28] F.V. Ferreira, F.S. Brito, W. Franceschi, E.A.N. Simonetti, L.S. Cividanes, M. Chipara, K. Lozano, Functionalized graphene oxide as reinforcement in epoxy based nanocomposites, Surf. Interface 10 (2018) 100–109.
[29] S. Sessarego, S.C.G. Rodrigues, Y. Xiao, Q. Lu, J.M. Hill, Phosphonium-enhanced chitosan for Cr (VI) adsorption in wastewater treatment, Carbohydr. Polym. 211 (2019) 249–256.
[30] J. Hee, S. Choi, Y. Bong, Geographical origin authentication of onions using stable isotope ratio and compositions of C, H, O, N, and S, Food Control 101 (2019) 121–125.
[31] E. Burresi, N. Taurisano, M.L. Protopapa, L. Latterini, M. Palmisano, L. Mirenghi, M. Schioppa, V. Morandi, R. Mazzaro, M. Penza, Influence of the synthesis conditions on the microstructural, compositional and morphological properties of graphene oxide sheets, Ceram. Int. (In Press, Corrected Proof) doi:https://doi.org/10.1016/j.ceramint.2020.05.222.
[32] C. Li, Z. Wu, H. Yang, L. Deng, X. Chen, Reduced graphene oxide-cyclodextrin-chitosan electrochemical sensor: effective and simultaneous determination of *o*- and *p*-nitrophenols, Sens. Actuators B Chem. 251 (2017) 446–454.
[33] H. Khawaja, E. Zahir, M. Asif, M. Arif, Graphene oxide, chitosan and silver nanocomposite as a highly effective antibacterial agent against pathogenic strains, Colloids Surfaces A 555 (2018) 246–255.
[34] D. Wang, W. Jiang, Preparation of chitosan-based nanoparticles for enzyme immobilization, Int. J. Biol. Macromol. 126 (2019) 1125–1132.
[35] C. Wang, Z. Zhang, B. Chen, L. Gu, Y. Li, S. Yu, Design and evaluation of galactosylated chitosan/graphene oxide nanoparticles as a drug delivery system, J. Colloid Interface Sci. 516 (2018) 332–341.
[36] X. Wang, H. Xie, Z. Wang, K. He, Graphene oxide as a pesticide delivery vector for enhancing acaricidal activity against spider mites, Colloids Surf. B: Biointerfaces 173 (2019) 632–638.
[37] J. Shah, M.R. Jan, Magnetic chitosan graphene oxide composite for solid phase extraction of phenylurea herbicides, Carbohydr. Polym. 199 (2018) 461–472.
[38] G. Srivastava, S. Walke, D. Dhavale, W. Gade, J. Doshi, R. Kumar, P. Doshi, Tartrate/tripolyphosphate as co-crosslinker for water soluble chitosan used in protein antigens encapsulation, Int. J. Biol. Macromol. 91 (2016) 381–393.
[39] L. Rui, M. Xie, B. Hu, L. Zhou, M. Saeeduddin, X. Zeng, Enhanced solubility and antioxidant activity of chlorogenic acid-chitosan conjugates due to the conjugation of chitosan with chlorogenic acid, Carbohydr. Polym. 170 (2017) 206–216.
[40] A. Chouljenko, A. Chotiko, V. Reyes, L. Alfaro, C. Liu, B. Dzandu, S. Sathivel, Application of water-soluble chitosan to shrimp for quality retention, Food Sci. Technol. 74 (2016) 571–579.
[41] S. Yadav, N. Goel, V. Kumar, S. Singhal, Graphene oxide as proficient adsorbent for the removal of harmful pesticides: comprehensive experimental cum DFT investigations, Anal. Chem. Lett. 9 (2019) 291–310.
[42] J. Chen, L. Zheng, X. Chen, Z. Wang, C. Li, Synthesis and characterization of water-soluble chitosan grafted with hydrophilic aliphatic polyester, Int. J. Biol. Macromol. 74 (2015) 433–438.
[43] T. Sato, S. Abe, S. Ito, T. Abe, Silk fibroin fiber for selective palladium adsorption: kinetic, isothermal and thermodynamic properties, J. Environ. Chem. Eng. 7 (2019) 102958.
[44] R.L. White, C.M. White, H. Turgut, A. Massoud, Z.R. Tian, Comparative studies on copper adsorption by graphene oxide and functionalized graphene oxide nanoparticles, J. Taiwan Inst. Chem. Eng. 85 (2018) 18–28.
[45] B. Zhang, W. Shi, S. Yu, Y. Zhu, R. Zhang, J. Hwa, Adsorption of anion polyacrylamide from aqueous solution by polytetrafluoroethylene (PTFE) membrane as an adsorbent: kinetic and isotherm studies, J. Colloid Interface Sci. 544 (2019) 303–311.
[46] C. Qi, L. Zhao, Y. Lin, D. Wu, Graphene oxide/chitosan sponge as a novel filtering material for the removal of dye from water, J. Colloid Interface Sci. 517 (2018) 18–27.
[47] W.S. Wan Ngah Kamari, Isotherm, kinetic and thermodynamic studies of lead and copper uptake by H_2SO_4 modified chitosan, Colloids Surf. B Biointerfaces 73 (2009) 257–266.